COMMUNICATIONS CHEMISTRY

ARTICLE

https://doi.org/10.1038/s42004-019-0133-4 OPEN

Rivastigmine and metabolite analogues with putative Alzheimer's disease-modifying properties in a *Caenorhabditis elegans* model

Satish N. Dighe[1], Eugenio De la Mora[2], Stephen Chan[1], Srinivas Kantham[1], Gawain McColl[3], Jared A. Miles[1], Suresh Kumar Veliyath[1], B. Yogi Sreenivas[1], Zeyad D. Nassar[1], Israel Silman[4], Joel L. Sussman[5], Martin Weik[2], Ross P. McGeary[6], Marie-Odile Parat[1], Xavier Brazzolotto[7] & Benjamin P. Ross[1]

The development of polyphenols as drugs for Alzheimer's disease (AD) is thwarted by their meagre brain availability due to instability and poor druglikeness. Here we describe the successful development of stable, druglike polyphenolic analogues of the current AD drug rivastigmine, that have high apparent blood-brain barrier permeabilities and multifunctional properties for AD treatment. The compounds inhibit cholinesterases and amyloid beta (Aβ) fibrillation, protect against $A\beta_{42}$-induced toxicity in vitro, and demonstrate efficacy in vivo in a transgenic *Caenorhabditis elegans* model expressing $A\beta_{42}$, with potencies similar to rivastigmine and natural polyphenols. The results suggest that a tertiary amine substituent is amenable for developing water-soluble, membrane-permeable polyphenols, and its incorporation adjacent to a hydroxy group is favourable for intramolecular hydrogen bonding that facilitates membrane permeability. Carbamylation of one hydroxy group protects the polyphenols from degradation and mostly improves their membrane permeability. These design strategies may assist in the development of polyphenol-based drugs.

[1] School of Pharmacy, The University of Queensland, Brisbane, QLD 4072, Australia. [2] Université Grenoble Alpes, CEA, CNRS, IBS, 38000 Grenoble, France. [3] The Florey Institute of Neuroscience and Mental Health, University of Melbourne, Melbourne, VIC 3010, Australia. [4] Department of Neurobiology, Weizmann Institute of Science, 76100 Rehovot, Israel. [5] Department of Structural Biology, Weizmann Institute of Science, 76100 Rehovot, Israel. [6] School of Chemistry and Molecular Biosciences, The University of Queensland, Brisbane, QLD 4072, Australia. [7] Institut de Recherche Biomédicale des Armées, Département de Toxicologie et Risques Chimiques, 91223 Brétigny sur Orge, France. Correspondence and requests for materials should be addressed to B.P.R. (email: b.ross1@uq.edu.au)

Alzheimer's disease (AD) is the most common cause of dementia, which is characterised by dysfunction in cognition and memory[1]. Worldwide, over 44 million people are currently living with dementia, and this number is predicted to increase to around 135 million by 2050[2]. According to the amyloid hypothesis, fibrillation of accumulating amyloid beta (Aβ) is the primary event associated with AD pathogenesis[3]. Consequently, inhibition of Aβ fibrillation is a prospective disease-modifying drug target for AD[4].

A class of molecules showing potent inhibition of Aβ fibrillation are natural polyphenols, such as (−)-epigallocatechin gallate (EGCG) and tannic acid[5–7]. However, the development of polyphenols as drugs for AD and other central nervous system (CNS) diseases is thwarted by their poor CNS availability[8]. This is understandable because many polyphenols do not comply with Lipinski's rule of five[9,10] or with CNS druglike criteria[11–14]. Furthermore, they are very susceptible to first-pass conjugative metabolism, and they contain metabolically unstable groups such as the ester linkages within EGCG and tannic acid[9,15]. Another substantial impediment to the delivery of polyphenols to their sites of action in vivo is their high propensity to oxidise to quinones, which are a class of compounds that have been associated with toxicity by acting as promiscuous electrophiles[16,17].

We now report the development of potent, druglike inhibitors of Aβ fibrillation, with estimated high blood–brain barrier (BBB) permeabilities, despite the molecules containing a polyphenolic pharmacophore such as pyrogallol or catechol. This was achieved by incorporating one or two additional hydroxy groups into the structure of the current AD drug, rivastigmine, and of its metabolite, NAP 226–90 (NAP) (Fig. 1a). Rivastigmine is a second-generation cholinesterase (ChE) inhibitor, which presents advantages compared to the first generation ones: it readily crosses the BBB; has minimal peripheral side effects; and pseudo-irreversibly inhibits both acetylcholinesterase (AChE) and butyrylcholinesterase (BuChE)[18,19]. The mechanism of action of rivastigmine involves carbamylation of the ChE active-site serine residue, with concomitant formation of the phenol NAP (Fig. 1a)[19]. We hypothesised that rivastigmine analogues containing one or two additional hydroxy groups on the aromatic ring could cross the BBB, and react with the ChE active-site serine residue, thereby releasing polyphenolic analogues of NAP (Fig. 1a). Furthermore, we hypothesised that these NAP analogues would possess the anti-Aβ fibrillation property of polyphenols such as EGCG. Although research has focussed on increasing the ChE inhibitory potential of rivastigmine[18,20–23], which would have a symptomatic effect in AD, no previous study has used the subtle change of only adding one or two hydroxy groups to the structures of rivastigmine or NAP as a basis for delivering potentially disease-modifying polyphenols to the brain. Moreover, this approach may create a multifunctional molecule, with anti-ChE activity residing in the rivastigmine analogue, and anti-Aβ fibrillation activity attributed to the NAP analogue, which would be released in vivo by the action of ChEs. Beneficially, the selectivity of rivastigmine for the G1 isoform of AChE[24] may promote polyphenolic NAP analogue release in the areas of the brain that are most affected by AD[23,25], as explained in the Supplementary Discussion. Another advantage of this strategy is that carbamylation of one of the phenolic hydroxy groups of the NAP analogues (thus forming rivastigmine analogues) may both protect the compounds from auto-oxidation and impede conjugative metabolism, which are undesirable traits that hinder the delivery of natural polyphenols.

Here, we communicate the design and synthesis of druglike polyphenolic analogues of rivastigmine and NAP. We describe their inhibitory effects on $A\beta_{42}$ fibrillation and ChE activity, and determine the X-ray crystal structures of both AChE and BuChE in complex with the most effective compound, demonstrating that the enzymes are carbamylated and release the active polyphenolic product. We characterise the BBB permeabilities and chemical stabilities of the most promising compounds, showing that some compounds have high permeability and good stability. Finally, we report that these compounds protect against $A\beta_{42}$-induced toxicity in both SH-SY5Y neuroblastoma cells in vitro and a transgenic $A\beta_{42}$-expressing *Caenorhabditis elegans* strain[26] in vivo.

Results

Synthesis of phenols 1–7. NAP analogues (Fig. 1b) containing one (**2**–**5**) or two (**6** and **7**) additional hydroxy groups compared to racemic NAP (**1**) were selected for synthesis. A new route for the synthesis of racemic NAP (**1**) was developed as described in Fig. 1c and in the Supplementary Discussion. A similar route was also used for the synthesis of NAP analogues **2**–**7** (Fig. 1d, Table 1 and Supplementary Discussion).

Effects of the phenols on Aβ fibrillation. After racemic NAP (**1**) and NAP analogues (**2**–**7**) had been synthesised, their effects on Aβ fibrillation were evaluated using fluorescent dyes, specifically thioflavin-T (ThT) and ProteoStat dye assays[27,28], as well as by transmission electron microscopy (TEM). The ThT assay kinetic traces for $A\beta_{42}$ fibril formation, alone and in the presence of compounds **1**–**7**, EGCG, and gallic acid, are shown in Fig. 2a. A characteristic sigmoidal kinetic accrual curve was observed[29], to which an empirical sigmoidal model was fitted and the amplitude obtained. The extent of fibrillation was estimated from the amplitude of each compound-treated sample, expressed relative to the control $A\beta_{42}$ amplitude, which represented 100% fibrillation (Fig. 2b). Figure 2 clearly shows that except for racemic NAP (**1**) and **4**, the compounds inhibit $A\beta_{42}$ fibrillation.

The results of the ThT assay were verified by estimating the extent of fibrillation at equilibrium with the ProteoStat dye[28] (Fig. 2c). Figure 2c illustrates that in the ProteoStat assay the compounds displayed similar effects to those observed using the ThT assay. The results of both fluorometric assays document that EGCG and **5** are very strong inhibitors of $A\beta_{42}$ fibrillation, while **2** and **3** are strong-to-moderate inhibitors. NAP analogues **6** and **7** showed relatively moderate-to-weak activity, while **4** and racemic NAP (**1**) do not inhibit $A\beta_{42}$ fibrillation.

TEM was used to study the effects of the compounds on the morphology of $A\beta_{42}$ aggregates after 42 h incubation at the end of the ThT experiment. The observed morphologies were consistent with the findings of the fluorometric assays. The $A\beta_{42}$ control showed dense clusters of fibrils (Fig. 2d), whereas $A\beta_{42}$ incubated with EGCG or gallic acid showed amorphous structures (Fig. 2e, f). TEM photomicrographs for NAP analogues (**2**–**6**) showed fibrils for **4** (Fig. 2i), amorphous structures for **5** (Fig. 2j), and a combination of fibrils and amorphous structures for **2**, **3** and **6** (Fig. 2g, h and k, respectively). It was further observed that incubation with **5** (Fig. 2j) resulted in amorphous structures very similar to those obtained after incubation with EGCG (Fig. 2e).

In terms of structure–activity relationships for inhibition of $A\beta_{42}$ fibrillation, di-hydroxy NAP analogues were better inhibitors than tri-hydroxy NAP analogues, with the exception of di-hydroxy compound **4**, which was inactive. For di-hydroxy analogues (**2**–**5**), when the additional hydroxy group was present at a *para* position (**5**) relative to the racemic NAP (**1**) hydroxy group, the compound was a very strong inhibitor, displaying activity that was more potent than that of gallic acid, and comparable to that of EGCG. When the additional hydroxy group was present at an *ortho* position (**2** and **3**) relative to the racemic NAP (**1**) hydroxy group, the molecules were strong-to-moderate

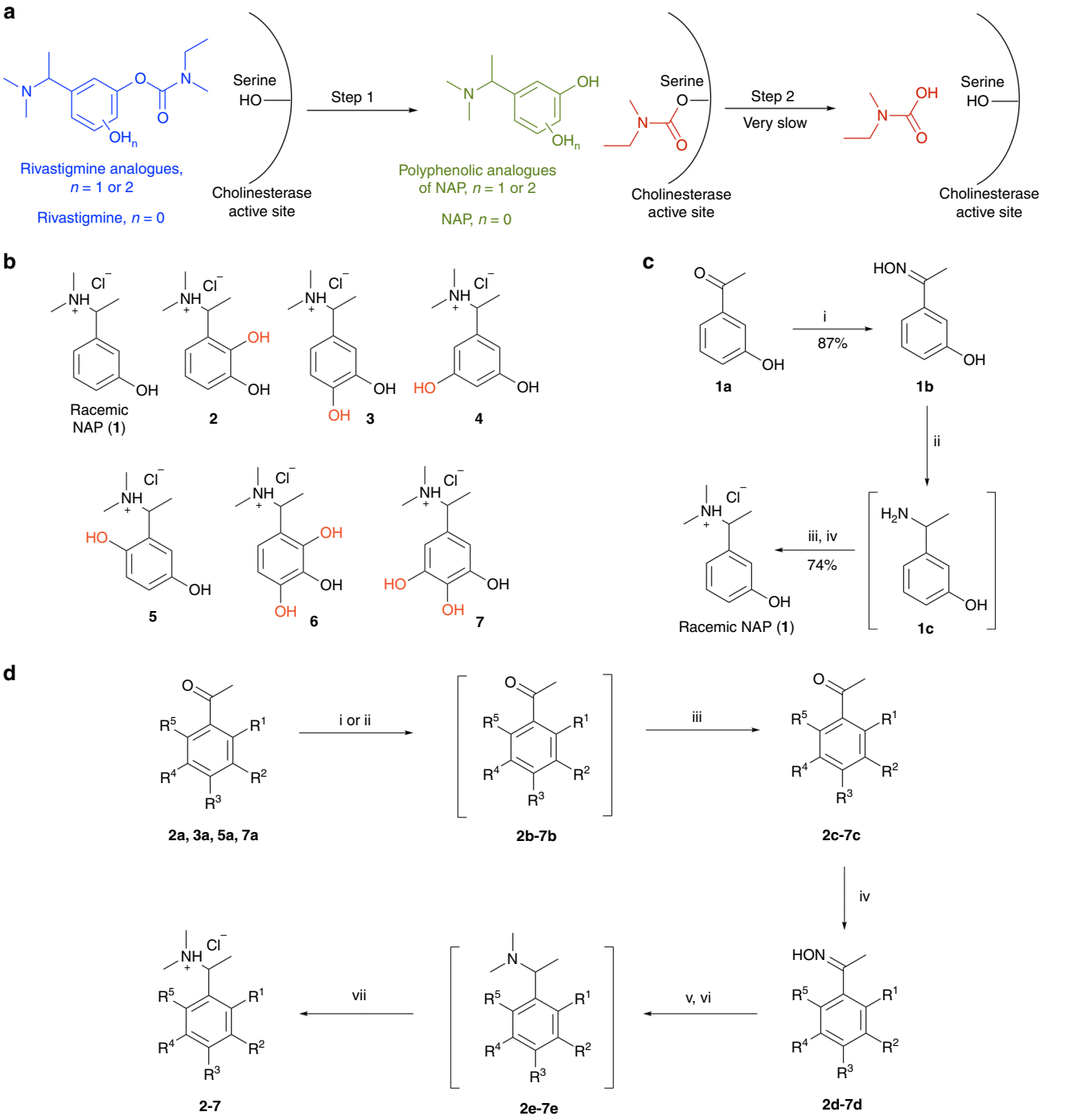

Fig. 1 Design concept for rivastigmine and NAP analogues as well as chemical structures and synthesis of phenols. **a** Hydrolysis of rivastigmine and designed rivastigmine analogues by cholinesterases (ChEs). We hypothesised that rivastigmine analogues containing one or two additional hydroxy groups on the aromatic ring would react with the ChE active-site serine, releasing polyphenolic analogues of NAP, which possesses the anti-Aβ fibrillation property of polyphenols such as epigallocatechin gallate (EGCG). The carbamylated serine is identical to that formed by rivastigmine; hence, we hypothesised that the rivastigmine analogues would also cause pseudo-irreversible inhibition of ChEs. **b** Chemical structures of racemic NAP (**1**) and NAP analogues (**2**–**7**). Red indicates hydroxy group/s added to the NAP structure. NAP 226–90 is the (*S*)-enantiomer of compound **1**. (**c**) Synthesis of racemic NAP (**1**) using a previously unreported synthetic route. Reagents and conditions: (i) $NH_2OH{\cdot}HCl$, triethylamine, MeOH, reflux; (ii) 10 wt % Pd/C, H_2, MeOH, rt; (iii) 10 wt% Pd/C, H_2, HCHO (40 vol % aq. solution), MeOH, rt; (iv) 32 wt% aq. HCl, MeOH, rt. **d** Synthesis of NAP analogues **2**–**7**. Reagents and conditions: (i) BF_3-etherate/NaI, MeCN, rt; (ii) BBr_3, CH_2Cl_2, −5 °C; (iii) TBDMS-Cl, DMAP, imidazole, CH_2Cl_2, 0 °C to rt; (iv) $NH_2OH{\cdot}HCl$, triethylamine, MeOH, reflux; (v) 10 wt% Pd/C, H_2, MeOH, rt; (vi) 10 wt% Pd/C, H_2, HCHO (40 vol % aq. solution), MeOH, rt; (vii) 32 wt% aq. HCl. MeOH, rt. Yields and substituents are described in Table 1

Table 1 Yields and substituents for the synthesis of NAP analogues 2–7 shown in Fig. 1d

Compounds	Yield (%)	R^1	R^2	R^3	R^4	R^5
2a	[a]	OCH_3	OCH_3	H	H	H
2b	[b]	OH	OH	H	H	H
2c	82[c]	OH	OTBDMS	H	H	H
2d	90	OH	OTBDMS	H	H	H
2e	[b]	OH	OTBDMS	H	H	H
2	27[c]	OH	OH	H	H	H
3a	[d]	H	OCH_3	OH	H	H
3b	[b]	H	OH	OH	H	H
3c	89[c]	H	OTBDMS	OTBDMS	H	H
3d	95	H	OTBDMS	OTBDMS	H	H
3e	[b]	H	OTBDMS	OTBDMS	H	H
3	42[c]	H	OH	OH	H	H
4b	[d]	H	OH	H	OH	H
4c	83	H	OH	H	OTBDMS	H
4d	84	H	OH	H	OTBDMS	H
4e	[b]	H	OH	H	OTBDMS	H
4	42[c]	H	OH	H	OH	H
5a	[d]	H	OCH_3	H	H	OH
5b	[b]	H	OH	H	H	OH
5c	88[c]	H	OTBDMS	H	H	OH
5d	89	H	OTBDMS	H	H	OH
5e	[b]	H	OTBDMS	H	H	OH
5	48[c]	H	OH	H	H	OH
6b	[d]	OH	OH	OH	H	H
6c	90	OH	OTBDMS	OTBDMS	H	H
6d	93	OH	OTBDMS	OTBDMS	H	H
6e	[b]	OH	OTBDMS	OTBDMS	H	H
6	12[c]	OH	OH	OH	H	H
7a	[d]	H	OCH_3	OCH_3	OCH_3	H
7b	[b]	H	OH	OH	OH	H
7c	90[c]	H	OTBDMS	OTBDMS	OTBDMS	H
7d	94	H	OTBDMS	OTBDMS	OTBDMS	H
7e	[b]	H	OTBDMS	OTBDMS	OTBDMS	H
7	11[c]	H	OH	OH	OH	H

[a]Substituted acetophenone **2a** was synthesised from *ortho*-vanillin as described in Supplementary Fig. 1
[b]Compound was not isolated
[c]Yield for two steps
[d]Substituted acetophenones **3a**, **5a**, **7a**, **4b** and **6b** were commercially available

inhibitors, equipotent with gallic acid but less active than EGCG. Moreover, when the hydroxy group was at the *meta* position (**4**) relative to the racemic NAP (**1**) hydroxy group, the compound was inactive. Overall, the results supported the hypothesis that the introduction of one or two additional hydroxy group/s into the racemic NAP (**1**) aromatic ring can produce analogues that inhibit $A\beta_{42}$ fibrillation, whereas racemic NAP (**1**) itself lacks this activity. At this point, compounds **2**, **3** and **5** emerged as promising $A\beta_{42}$ fibrillation inhibitors among the series of synthesised compounds (**1**–**7**).

Estimation of the BBB permeabilities of the phenols. An MDR1-MDCKII cell-based model[30,31] was used to estimate the BBB permeabilities of the $A\beta_{42}$ fibrillation inhibitors, NAP analogues **2**, **3** and **5**, as well as a series of reference compounds including the natural polyphenols EGCG and gallic acid. Table 2 shows the apparent permeability (P_{app}) values and permeability categories for the compounds. Propranolol[32], metoprolol, and the current approved AD drugs (*S*)-rivastigmine, donepezil, and galantamine were used as high permeability reference compounds. Nadolol, fenoterol, and digoxin were used as low permeability reference compounds, and digoxin was also a marker of P-glycoprotein (P-gp) efflux[32]. Although EGCG and gallic acid are very good inhibitors of $A\beta_{42}$ fibrillation in vitro, the MDR1-MDCKII cell-based model shows that they have very low permeabilities (P_{app} values even lower than nadolol, fenoterol and digoxin)[32], suggesting that they cross the BBB very poorly, thus preventing their use as drugs for AD. Remarkably, racemic NAP (**1**), **2** and **5** showed high permeabilities, while **3** had moderate permeability bordering on the low permeability category. This indicates that the effect on P_{app} of adding one hydroxy group onto the aromatic ring of racemic NAP (**1**) can vary substantially depending on the exact position of the additional hydroxy group. When the additional hydroxy group was *ortho* to the alkyl amino group of racemic NAP (**1**) (compounds **2** and **5**), the P_{app} was practically unaffected; however, when the additional hydroxy group was *para* to the alkyl amino group of racemic NAP (**1**) (compound **3**), the P_{app} was substantially reduced. In silico modelling predicted that the lowest energy conformations of **2** and **5** each contain an intramolecular hydrogen bond between the additional hydroxy group and the adjacent tertiary amine (Supplementary Table 6). This bond would promote the membrane permeability of **2** and **5** by concealing their polar hydroxy and tertiary amine groups[33]. In contrast, intramolecular hydrogen bonding is not predicted for **3** in which the additional hydroxy group is distant to the tertiary amine (Supplementary Table 6), possibly explaining why its membrane permeability is inferior to **2** and **5**. Compound **3** is also predicted to be more hydrophilic than **2** and **5**, further explaining its lower membrane permeability (compound **3** has a larger solvent accessible hydrophilic surface area and a lower octanol-water partition coefficient than **2** and **5**,

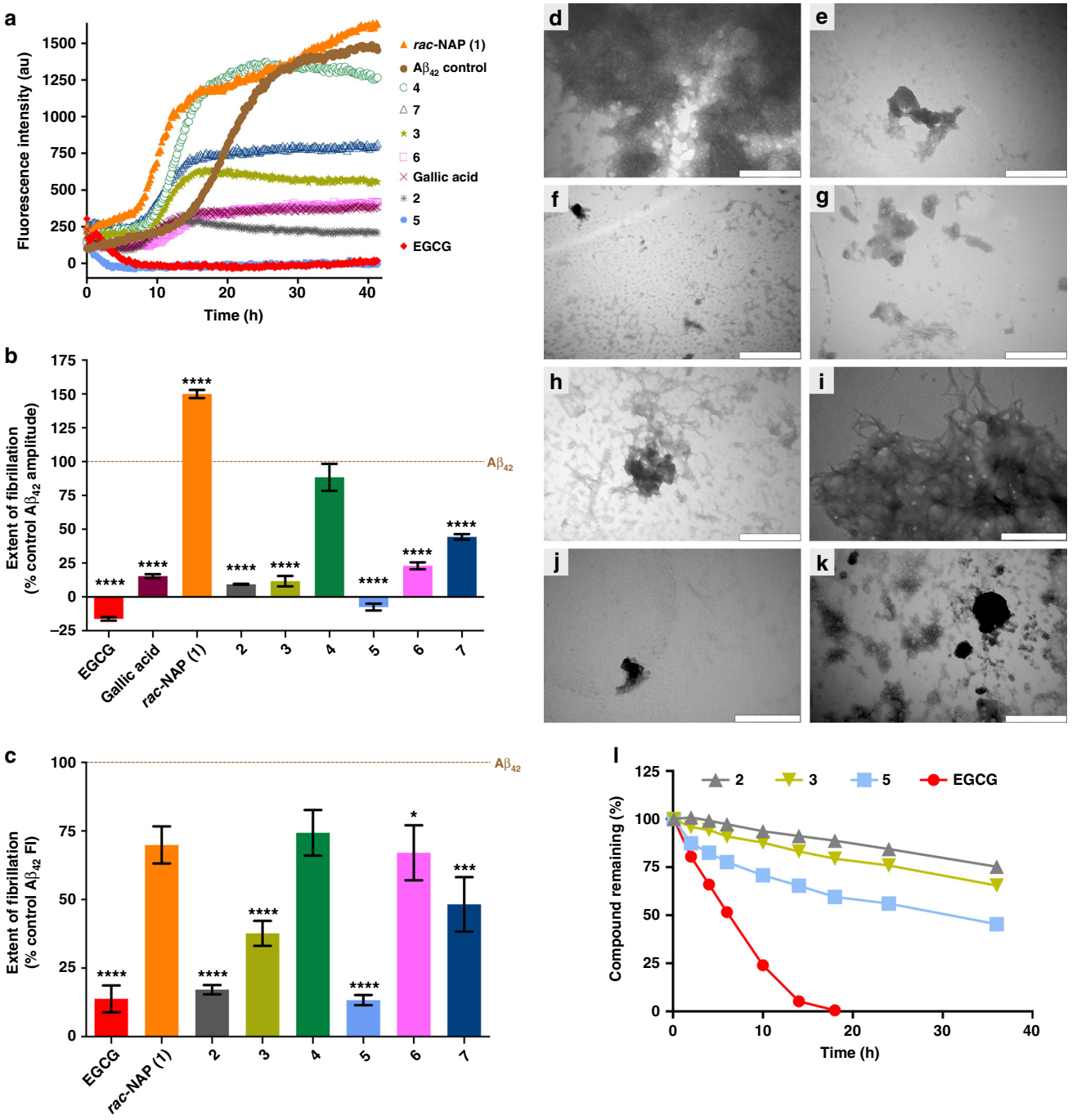

Fig. 2 Effects of phenols on $A\beta_{42}$ fibrillation and chemical stabilities of phenols. **a**, **b** $A\beta_{42}$ fibrillation monitored by in situ ThT fluorescence. $A\beta_{42}$ (30 μM) was incubated alone or with **1**–**7**, epigallocatechin gallate (EGCG) or gallic acid (100 μM) in pH 7.4 phosphate buffer containing 20 μM ThT, at 37 °C under quiescent conditions. **a** Representative kinetic plots corrected for the fluorescence of ThT alone (20 μM). Fluorescence readings (λ_{ex} 440 nm, λ_{em} 480 nm) were recorded every 10 min. **b** Extent of fibrillation depicted as % of the $A\beta_{42}$ control amplitude. Values are the mean ± SEM of at least three independent experiments with $^{****}p < 0.0001$ c.f. $A\beta_{42}$ control as determined by one-way analysis of variance (ANOVA) followed by Tukey's multiple comparisons test. **c** $A\beta_{42}$ fibrillation estimated by ProteoStat fluorescence. $A\beta_{42}$ (30 μM) was incubated alone or with compounds **1**–**7** or EGCG (100 μM) in pH 7.4 phosphate buffer, at 37 °C under quiescent conditions for 42 h. ProteoStat dye was then added, and the fluorescence intensity was recorded (λ_{ex} 544 nm, λ_{em} 590 nm). The extent of fibrillation is depicted as % of the $A\beta_{42}$ control fluorescence intensity. Values are the mean ± SEM of three independent experiments with $^{*}p < 0.05$, $^{***}p < 0.001$ and $^{****}p < 0.0001$ c.f. $A\beta_{42}$ control as determined by one-way ANOVA followed by Tukey's multiple comparisons test. **d**–**k** TEM images of samples collected at the end of the ThT experiment (42 h incubation). All scale bars indicate 500 nm $A\beta_{42}$ (30 μM) incubated alone (**d**) and with 100 μM of: **e** EGCG; **f** Gallic acid; **g** Compound **2**; **h** Compound **3**; **i** Compound **4**; **j** Compound **5**; **k** Compound **6**. **l** Chemical stabilities of EGCG, **2**, **3** and **5**. Time course showing estimated % compound remaining for compounds incubated over 36 h in pH 7.4 phosphate buffer at 23 °C

Table 2 Estimated BBB permeabilities

Compounds[a]	Mean P_{app}(10^{-6} cm/s)	Pgp efflux ratio	Permeability category[b]
Gallic acid[c]	0.01	29.3	Low
3,4-Dihydroxybenzoic acid	<0.03	[d]	Low
Epigallocatechin gallate (EGCG)[c]	0.07	2.97	Low
3-Hydroxybenzoic acid	<0.08	[d]	Low
2,3-Dihydroxybenzoic acid	<0.09	[d]	Low
Digoxin[c]	0.10	78.5	Low
2,5-Dihydroxybenzoic acid	<0.21	[d]	Low
Fenoterol[c]	0.22	[d]	Low
Nadolol	0.65	[d]	Low
3	1.13	0.88	Moderate
Galantamine	18.4	0.97	High
Metoprolol	20.4	[d]	High
Propranolol[c]	21.1	[d]	High
2	23.9	0.94	High
Donepezil	24.1	0.82	High
Racemic NAP (**1**)	25.8	0.80	High
5	26.3	0.85	High
(*S*)-Rivastigmine [(*S*)-**8**]	34.5	0.75	High

[a]Values are mean of at least two independent experiments using an MDR1-MDCKII cell-based model. Replicate P_{app} values were within 5% of the mean for high and moderate permeability compounds, and within 20% of the mean for low permeability compounds. The test concentration was 2 μM with 2.5 h incubation
[b]Low permeability: $P_{app} \leq 1.0$ ($\times 10^{-6}$ cm/s); Moderate permeability: $1.0 < P_{app} < 5.5$ ($\times 10^{-6}$ cm/s); High permeability: $P_{app} \geq 5.5$ ($\times 10^{-6}$ cm/s). The boundaries for low and high permeability categories are equivalent to 50 and 80% of the calculated fraction absorbed (Fa) in humans
[c]Data for these reference compounds was recently published[32]
[d]Not determined

according to calculated QikProp FISA and QPlogPo/w descriptors, Supplementary Table 7). Interestingly, an intramolecular hydrogen-bonding motif similar to that predicted for **2** and **5** exists in α-aminocresol antimalarial compounds, including the drug amodiaquine[34–36].

The P_{app} values of racemic NAP (**1**), **2**, **3** and **5** were 38- to 324-fold greater than the P_{app} values of poorly permeable matched pair compounds containing a carboxylic acid group in place of the alkyl amino group (Table 2). These differences in permeabilities can be explained by the predicted higher hydrophilicities and degrees of ionisation of the acids, which had larger solvent accessible hydrophilic surface areas, no solvent accessible hydrophobic surface areas, substantially lower octanol-water partition coefficients, and stronger pK_a values compared with the matched amines (based on the calculated QikProp FISA, FOSA, and QPlogPo/w descriptors, and Epik pK_a values, Supplementary Table 7). The literature indicates that basic aliphatic amines are a common feature of CNS drugs with good brain availability, unlike carboxylic acids, which are generally associated with poor brain availability and are uncommon in CNS drugs[12–14]. This knowledge combined with our results suggests that a tertiary amine group is preferred to a carboxylic acid group for developing water-soluble, membrane-permeable polyphenols, and its incorporation adjacent to a hydroxy group is favourable for intramolecular hydrogen bonding that facilitates membrane permeability.

Chemical stabilities of the phenols. Phenols that contain two hydroxy groups either *ortho* or *para* to each other are susceptible to auto-oxidation into *ortho*- and *para*-quinones, respectively[37]. This includes natural polyphenols that contain catechol and pyrogallol moieties[38,39]. The chemical stabilities of $A\beta_{42}$ fibrillation inhibitors **2**, **3** and **5**, as well as of EGCG, were studied in pH 7.4 phosphate buffer over 36 h (Fig. 2l). Solutions were placed into high-performance liquid chromatography (HPLC) autosampler vials that were sealed with PTFE/silicone septa and the headspace was air. Samples were analysed by reversed-phase (RP)-HPLC after 5 min, 2, 4, 6, 10, 14, 18, 24 and 36 h. EGCG completely degraded within 18 h. NAP analogue **5** degraded at a faster rate than **2** and **3**, which displayed similar profiles; however, the degradation of these three compounds (**2**, **3**, and **5**) was much slower than that of EGCG, with 75% of **2**, 66% of **3** and 45% of **5** remaining after 36 h. Although **2**, **3** and **5** are relatively more stable than EGCG, they nevertheless exhibited substantial degradation under the test conditions. We hypothesised that this liability could be overcome by carbamylation of one of their hydroxy groups, thus forming rivastigmine analogues that are less susceptible to auto-oxidation. Furthermore, as discussed above, the rivastigmine analogues may offer advantages in terms of BBB permeability, ChE inhibition, and release of the NAP analogue in the AD-affected brain. Hence, we proceeded to synthesise rivastigmine analogues **9**–**12**, and racemic rivastigmine (**8**).

Synthesis of carbamates 8–12. The chemical structures of rivastigmine analogues **9**–**12**, and of racemic rivastigmine (**8**) are shown in Fig. 3a. Each of these molecules (**8**–**12**) is the carbamylated form of a corresponding phenol, as listed here (phenol, carbamate): **1**, **8**; **2**, **9**; **3**, **10**; **5**, **11**; and **6**, **12**. Carbamylated derivatives of **4** and **7** were not synthesised because **4** did not inhibit $A\beta_{42}$ fibrillation and **7** was a relatively weak inhibitor. The synthesis of racemic rivastigmine (**8**) is described in Fig. 3b and in the Supplementary Discussion.

For the synthesis of rivastigmine analogues **9**–**12**, it was necessary to selectively carbamylate only the hydroxy group corresponding to the NAP hydroxy group; therefore, an orthogonal protecting group strategy was developed as described in Fig. 4, Supplementary Figs. 2 and 3, and the Supplementary Discussion.

Effects of the carbamates on Aβ fibrillation. The effects of (*S*)-rivastigmine [(*S*)-**8**] and the rivastigmine analogues (**9**–**12**) on Aβ fibrillation was evaluated using ThT and ProteoStat dye assays, as well as TEM (Supplementary Figs. 18–20). Just like its phenolic counterpart (**1**), (*S*)-rivastigmine [(*S*)-**8**] did not inhibit $A\beta_{42}$ fibrillation. Rivastigmine analogue **11** was also inactive, in contrast to the corresponding NAP analogue (**5**), which was a very strong $A\beta_{42}$ fibrillation inhibitor. Rivastigmine analogues **9** and **10** displayed relatively moderate-to-weak activity, and were *ca.*

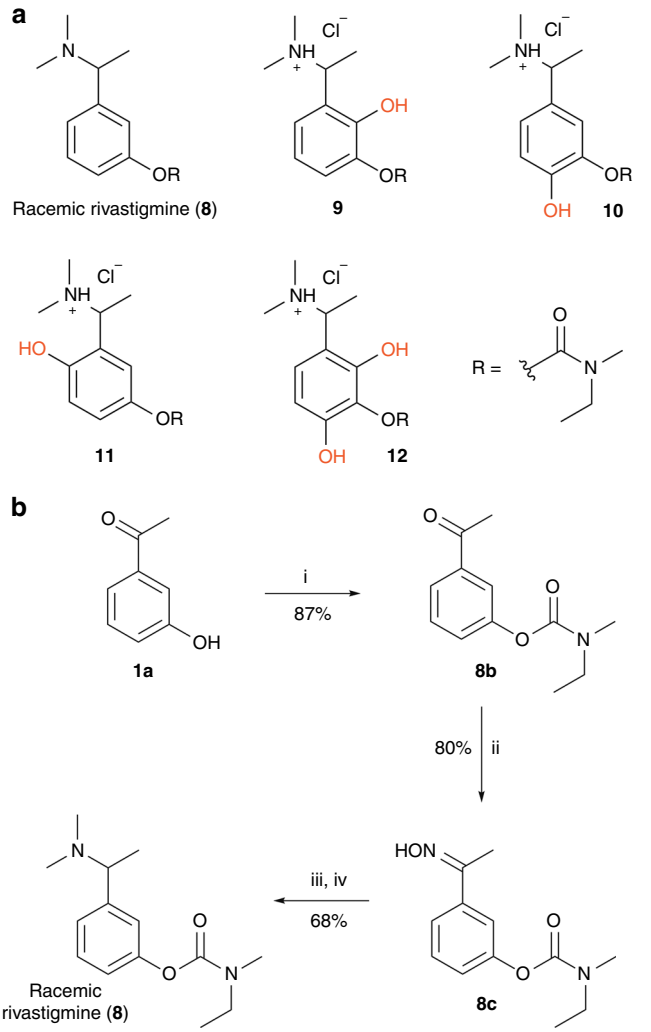

Fig. 3 Chemical structures of carbamates and synthesis of racemic rivastigmine. **a** Chemical structures of racemic rivastigmine (**8**) and rivastigmine analogues (**9–12**). Red indicates hydroxy group/s added to the rivastigmine structure. The drug rivastigmine is the (*S*)-enantiomer of compound **8**, and is referred to as (*S*)-rivastigmine [(*S*)-**8**] in this study. **b** Synthesis of racemic rivastigmine (**8**). Reagents and conditions: (i) ethyl (methyl)carbamic chloride, KOH, toluene, reflux; (ii) $NH_2OH{\cdot}HCl$, triethylamine, MeOH, reflux; (iii) 10 wt% Pd/C, H_2, MeOH, rt; (iv) 10 wt% Pd/C, H_2, HCHO (40 vol % aq. solution), MeOH, rt

2–4-fold less potent than the corresponding NAP analogues **2** and **3**, respectively. Thus, carbamylation of **2**, **3** and **5**, the most promising $A\beta_{42}$ fibrillation inhibitors among the NAP analogues series (**2**–**7**), results in the formation of rivastigmine analogues (**9**–**11**) with little or no direct effects on $A\beta_{42}$ fibrillation. Therefore, the rivastigmine analogues (**9**–**11**) have the potential to be prodrugs of $A\beta_{42}$ fibrillation inhibitors (NAP analogues **2**, **3** and **5**).

Inhibition of ChEs by the carbamates. Our strategy involved release of potentially disease-modifying NAP analogues in vivo, upon decarbamylation of their respective rivastigmine counterparts by the different ChEs (Fig. 1a). This process would encompass carbamylation of the ChE active-site serine residue, causing pseudo-irreversible inhibition of the enzyme[23]. ChE inhibition is an important symptomatic drug target for AD, and three of the four currently available drugs (donepezil, galantamine, and rivastigmine) are based on this target. Therefore, rivastigmine analogues **9**–**11** were evaluated in vitro for human acetylcholinesterase (huAChE) and human butyrylcholinesterase (huBuChE) inhibitory activity. Racemic rivastigmine (**8**) and (*S*)-rivastigmine [(*S*)-**8**] were included as positive control benchmark compounds. Compound **12** was not included because it only weakly inhibited equine BuChE and *Electrophorus electricus* AChE in preliminary screening studies (Supplementary Table 4), and IC_{50} values could not be obtained. Results for inhibition of huChEs are shown in Table 3. All studied compounds [(*S*)-**8**, **8**–**11**] displayed strong-to-moderate inhibition of huAChE and huBuChE. Racemic rivastigmine (**8**) was around twofold less potent than (*S*)-rivastigmine [(*S*)-**8**], probably because it contained *ca.* 50% of the relatively inactive R-enantiomer[19]. All of the rivastigmine analogues (**9**–**12**) were racemic mixtures, so comparison of their activity with racemic rivastigmine (**8**) is more appropriate than comparison with (*S*)-rivastigmine [(*S*)-**8**]. Rivastigmine analogues **9**–**11** were less potent than racemic rivastigmine (**8**) by a factor of 2.9-to-18.5, with **10** and **11** having similar potency to each other, which was superior to **9**.

The results shown in Table 3 and Supplementary Table 4 are based on a 40 min period of incubation of compound with enzyme prior to measuring ChE activity. The effects of varying the incubation time on ChE activity is shown in Fig. 5a, b for **11** and in Supplementary Fig. 21 for rivastigmine (**8**) and (*S*)-rivastigmine [(*S*)-**8**]. The IC_{50} values of these compounds decreased as the incubation time increased; this progressive inhibition is consistent with pseudo-irreversible carbamylation of the enzyme's active-site serine[19].

X-ray crystallographic studies. To confirm that inhibition is caused by carbamylation of the catalytic serine conserved in all ChEs, we determined the three-dimensional structures of *Torpedo californica* AChE (*Tc*AChE) and huBuChE upon incubation with **11**, the most promising compound at this stage. *Tc*AChE is an accepted model of huAChE due to high structural similarity. The structures refined at 2.05 Å resolution for *Tc*AChE (PDB ID: 6EUE; Fig. 5c and Supplementary Fig. 22a), at 2.60 Å for huBuChE produced in Chinese hamster ovary cells (huBuChE-CHO, PDB ID: 6EYF; Fig. 5d and Supplementary Fig. 22b), and at 2.70 Å for huBuChE produced in insect cells ($huBuChE_{insect}$, PDB ID: 6EZ2, not shown), unequivocally show that **11** carbamylates the catalytic serine within the active-site gorge. In contrast to the structure of the rivastigmine-*Tc*AChE complex (PDB ID: 1GQR)[19], we do not observe a NAP analogue (**5**) bound in the active-site. Its position is occupied by a PEG molecule (Supplementary Fig. 22a), as frequently seen in AChE structures obtained from crystals when using PEG as the precipitant. The presence of PEG instead of **5** shows that the product (**5**) is released from the active-site gorge and is free to diffuse into inter-synaptic space to act as an anti-Aβ fibrillation agent. Additionally, for *Tc*AChE, we observed two alternative conformations for Phe330 (Supplementary Fig. 22a) and His440 (Fig. 5c), the latter belonging to the catalytic triad. Compared to the native structure, the His440 side chain is displaced from its most stable conformation by the carbamoyl moiety of Ser200. In BuChE structures, extra electron density was observed inside the gorge. While this density was difficult to assign in the $huBuChE_{insect}$ structure, it was obvious that it corresponds to an additional molecule of **11** in the $huBuChE_{CHO}$ structure (Supplementary Fig. 22b). The presence of this molecule is certainly due to the high compound concentration used during co-crystallisation. Nevertheless, the potential release of the NAP analogue (**5**) from the active-site gorge was demonstrated. All X-ray crystal structures confirm the

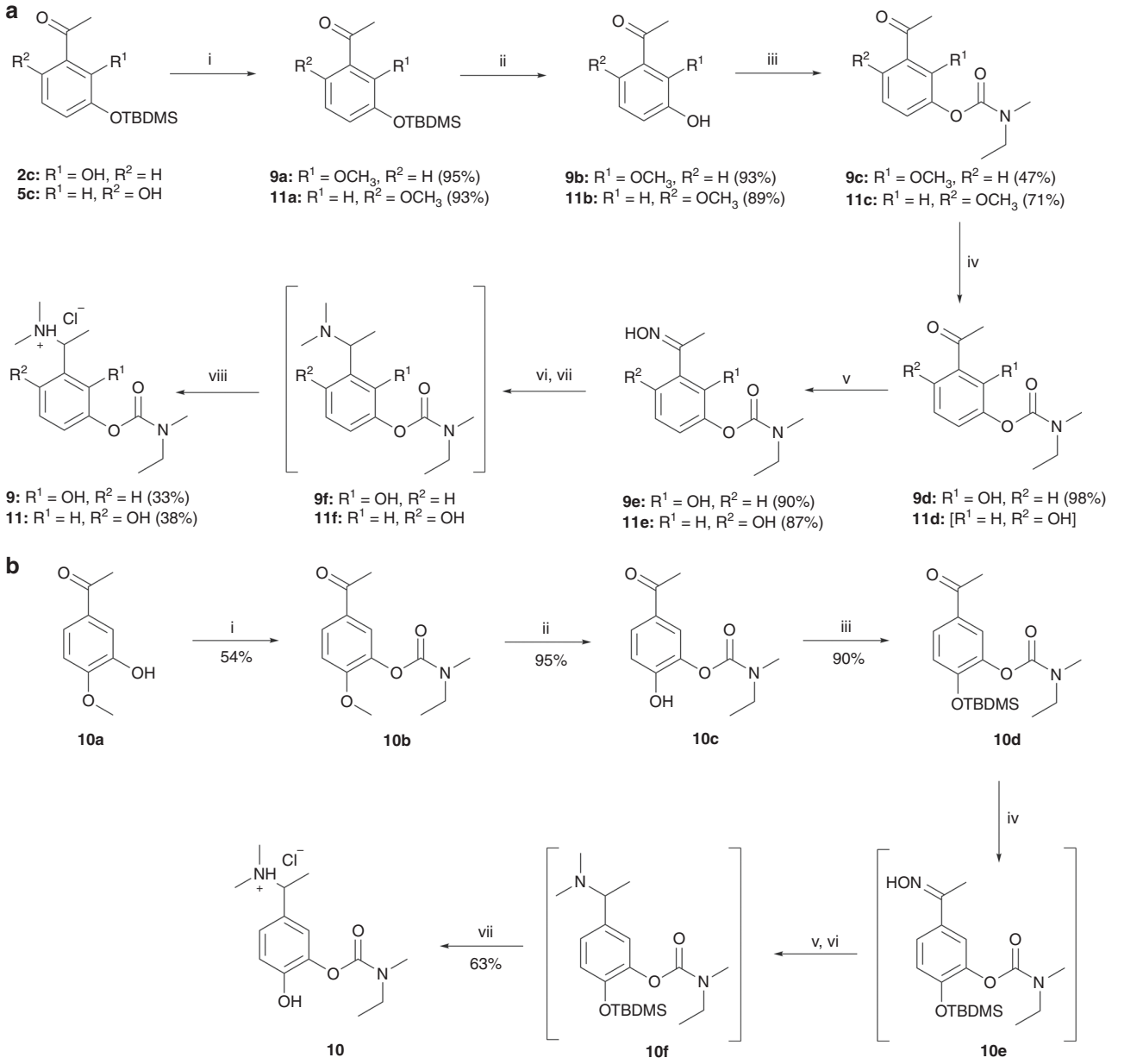

Fig. 4 Synthesis of rivastigmine analogues **9**–**11**. **a** Synthesis of **9** and **11**. Reagents and conditions: (i) CH_3I, K_2CO_3, MeCN, rt; (ii) 32 wt% aq. HCl, MeOH, rt; (iii) ethyl(methyl)carbamic chloride, KOH, toluene, reflux; (iv) BBr_3, CH_2Cl_2, −5 °C; (v) $NH_2OH{\cdot}HCl$, triethylamine, MeOH, reflux; (vi) 10 wt% Pd/C, H_2, MeOH, rt; (vii) 10 wt% Pd/C, H_2, HCHO (40 vol % aq. solution), MeOH, rt; (viii) 32 wt% aq. HCl, MeOH, rt. The synthesis of **2c** and **5c** is described in Fig. 1d. **b** Synthesis of **10**. Reagents and conditions: (i) Ethyl(methyl)carbamic chloride, KOH, toluene, reflux; (ii) BBr_3, CH_2Cl_2, −5 °C; (iii) TBDMS-Cl, DMAP, imidazole, CH_2Cl_2, 0 °C to rt; (iv) $NH_2OH{\cdot}HCl$, triethylamine, MeOH, reflux; (v) 10 wt% Pd/C, H_2, MeOH, rt; (vi) 10 wt% Pd/C, H_2, HCHO (40 vol % aq. solution), MeOH, rt; (vii) 32 wt% aq. HCl, MeOH, rt. The synthesis of acetophenone **10a** is described in Supplementary Fig. 2

potential of **11** to act as a multifunctional molecule with inherent ChE inhibition, as well as being a prodrug of **5**, which is released by the action of ChEs and inhibits Aβ fibrillation.

Estimation of the BBB permeabilities of the carbamates. The MDR1-MDCKII cell-based model was used to estimate the BBB permeabilities of racemic rivastigmine (**8**) and rivastigmine analogues (**9**–**11**) (Table 4), with reference compounds included for comparison (Tables 2 and 4). All the carbamates (**8**–**11**) had high permeabilities, with **8**, **9** and **11** even more permeable than the reference compounds, propranolol, metoprolol and galantamine. There was no meaningful difference between the permeabilities of (*S*)-rivastigmine [(*S*)-**8**] and racemic rivastigmine (**8**), indicating that stereochemistry does not affect the transport of rivastigmine across the MDR1-MDCKII cell monolayer, which probably occurs via passive transcellular diffusion. The permeability of carbamate **9** was similar to that of the corresponding phenol **2**, whereas for carbamates **8**, **10** and **11** the permeabilities were 1.3-fold, 8.1-fold and 1.3-fold greater than for the corresponding phenols **1**, **3** and **5**, respectively. Thus, carbamylation of a phenolic hydroxy group in this series of compounds can either enhance or have very little effect on BBB permeability, which is generally consistent with carbamylation decreasing the hydrophilicity of the compounds (compared to the phenols the carbamates had smaller solvent accessible hydrophilic surface areas, larger solvent accessible hydrophobic surface areas, and higher octanol-water partition coefficients, according to calculated

Table 3 In vitro inhibition of human cholinesterases

Compounds	HuAChE IC_{50} Mean ± SEM (μM)[a,b]	HuBuChE IC_{50} Mean ± SEM (μM)[a,b]
(*S*)-Rivastigmine [(*S*)-**8**]	6.33 ± 0.45 (0.48)	0.804 ± 0.045 (0.63)
Racemic rivastigmine (**8**)	13.2 ± 2.3 (1.0)	1.27 ± 0.02 (1.0)
9	131 ± 5 (9.9)	23.5 ± 3.9 (18.5)
10	38.1 ± 4.4 (2.9)	9.81 ± 0.06 (7.7)
11	38.1 ± 1.7 (2.9)	8.91 ± 0.42 (7.0)

[a]Values are mean ± SEM of at least three independent experiments. Values in parentheses are IC_{50} relative to racemic rivastigmine (**8**) (IC_{50} compound/IC_{50} **8**)
[b]IC_{50} was calculated with a 40 min incubation of compound with enzyme prior to adding acetylthiocholine iodide

QikProp FISA, FOSA and QPlogPo/w descriptors, Supplementary Table 7). Compounds **9**–**11** each contain one more hydroxy group than rivastigmine, and the exact position of the additional hydroxy group on the aromatic ring affected P_{app} in a similar manner to that observed previously for NAP analogues **2**, **3** and **5**. Specifically, when the additional hydroxy group was *para* to the alkyl amino group of racemic rivastigmine (**8**) (compound **10**), intramolecular hydrogen bonding between these two distant polar groups was impossible (confirmed by in silico modelling, Supplementary Table 6) and the P_{app} was substantially reduced, although **10** was nevertheless highly permeable. When the additional hydroxy group was *ortho* to the alkyl amino group of racemic rivastigmine (**8**) (compounds **9** and **11**), intramolecular hydrogen bonding (Supplementary Table 6) concealed the polarity of these two adjacent groups[33] and the P_{app} was less affected, with the P_{app} of **11** essentially identical to the P_{app} of racemic rivastigmine (**8**) while that of **9** decreased by one-third but was still well within the high permeability category.

The P_{app} value of racemic rivastigmine (**8**) was 9.3-fold greater than the P_{app} value of its moderately permeable matched pair compound containing a carboxylic acid group in place of the alkyl amino group, 3-((ethyl(methyl)carbamoyl)oxy)benzoic acid (Table 4). This difference in permeability can be explained by the predicted higher hydrophilicity and degree of ionisation of the acid, which had a larger solvent accessible hydrophilic surface area, a smaller solvent accessible hydrophobic surface area, a lower octanol-water partition coefficient, and a stronger pKa, compared with racemic rivastigmine (**8**) (based on the calculated QikProp FISA, FOSA, and QPlogPo/w descriptors and Epik pK_a, Supplementary Table 7). This confirms the earlier result for the NAP analogues showing that, in general, tertiary amines are preferred to carboxylic acids when developing water-soluble, membrane-permeable compounds.

Chemical stabilities of the carbamates. Previously, NAP analogues **2**, **3** and **5** were found to undergo substantial degradation in pH 7.4 phosphate buffer (Fig. 2l), and we hypothesised that this liability could be overcome by carbamylation of one of their hydroxy groups, thus forming rivastigmine analogues **9**–**11**. The chemical stabilities of **9**–**11** were studied in pH 7.4 phosphate buffer over 36 h (Fig. 6a–c). Solutions were placed into HPLC autosampler vials that were sealed with PTFE/silicone septa and the headspace was air. Samples were analysed over the 36 h period by RP-HPLC-high-resolution mass spectrometry (HRMS). Rivastigmine analogue **11** was stable under these conditions over the entire 36 h period (Fig. 6a), demonstrating that carbamylation of one of the two hydroxy groups of **5** protects it from degradation. Incubation of rivastigmine analogue **10** resulted in the rapid formation of an equilibrium mixture, apparently comprising **10** and its structural isomer **10i**, produced by intramolecular transfer of the carbamoyl group of **10** to the adjacent hydroxy group (Fig. 6b). Only a small amount of NAP analogue **3** was released from **10** and **10i** over the 36 h period (Fig. 6b), signifying that carbamates **10** and **10i** are quite stable to hydrolysis (Fig. 6a, **10** + **10i**). Similarly to what was observed for **10**, incubation of rivastigmine analogue **9** also rapidly produced an equilibrium mixture, apparently comprising **9** and its structural isomer **9i**, produced by intramolecular transfer of the carbamoyl group of **9** to the adjacent hydroxy group (Fig. 6c). A moderate amount of NAP analogue **2** was released from **9** and **9i** progressively over the 36 h period (Fig. 6c), indicating that carbamates **9** and **9i** are less stable to hydrolysis than **10** and **10i** (Fig. 6a, **9** + **9i** c.f. **10** + **10i**). Overall, carbamylation protected the NAP analogues (**2**, **3** and **5**) from degradation, with carbamate **11** being completely stable (Fig. 6a), and carbamates **9** and **10** releasing only low-to-moderate amounts of NAP analogues (Fig. 6b, c), which are inherently more stable over 36 h than the natural polyphenol EGCG (Fig. 2l).

Protection against Aβ-induced neurotoxicity in vitro. According to the amyloid hypothesis, the accumulation and fibrillation of Aβ are the primary events in AD pathogenesis[3,40], and soluble oligomeric forms of Aβ are highly neurotoxic[41]. The ability of the compounds (**1**–**6**, [(*S*)-**8**], **9**–**11**, EGCG) to protect neurons from $Aβ_{42}$-induced toxicity was assessed using SH-SY5Y neuroblastoma cells. $Aβ_{42}$ (30 μM) alone, or in combination with compounds (38 μM), was incubated in pH 7.4 phosphate buffer at 37 °C for 2 h, then added to SH-SY5Y cells, and incubated for 48 h at 37 °C. The final concentrations of $Aβ_{42}$ and of the compounds that the cells were exposed to were 3.9 and 5.0 μM, respectively. Cell viability was estimated by the 3-(4,5-dimethylthiazol-2-yl)-2,5-diphenyltetrazolium bromide (MTT) assay, and the results are shown in Fig. 6d. $Aβ_{42}$ alone was toxic to the cells, resulting in only 32% cell viability. NAP analogues **2**, **3**, **5** and **6** protected the cells from $Aβ_{42}$-induced toxicity, with cell viability being significantly higher, at 46–49% (**2**, **3** and **6**: $p < 0.05$; **5**: $p < 0.01$; c.f. $Aβ_{42}$ control), although this outcome was inferior to the protection afforded by EGCG, which allowed 75% cell viability ($p < 0.0001$ c.f. $Aβ_{42}$ control). The activity of these compounds (**2**, **3**, **5**, **6** and EGCG) was aligned with the results of earlier experiments demonstrating their ability to inhibit $Aβ_{42}$ fibrillation. Interestingly, racemic NAP (**1**), NAP analogue **4**, (*S*)-rivastigmine [(*S*)-**8**], and the rivastigmine analogues (**9**–**11**) did not protect the cells from $Aβ_{42}$-induced toxicity, which was consistent with their weak activity or complete inability to inhibit $Aβ_{42}$ fibrillation in previous experiments. The inherent toxicity of the compounds alone was examined under the same conditions, and *ca.* 70% cell viability or more was observed when cells were exposed to these compounds at 5 μM (Supplementary Fig. 23).

Protection against Aβ-induced toxicity in vivo. The protective effects of the compounds (**1**–**3**, **5**, **9**, **10**, **11**, (*S*)-**8** and EGCG) against Aβ-induced toxicity in vivo, was examined using the transgenic GMC101 strain of *C. elegans* in which the expression of full length $Aβ_{42}$ in body wall muscle cells induces paralysis within 48 h at 25 °C[42]. Strain CL2122 was used as a transgenic control and does not express Aβ[42,43]. Figure 6e shows the fraction of nematodes not paralysed after 16, 20 and 24 h at 25 °C, for untreated strains GMC101 and CL2122, and GMC101 grown on media that was pre-treated with 100 μL of 2 mM compound (**1**–**3**, **5**, **9**, **10**, **11**, (*S*)-**8** or EGCG)[26]. The control strain CL2122 exhibited no paralysis over the time course of the experiment, whereas *C. elegans* GMC101 expressing $Aβ_{42}$ showed a time-dependent paralysis[26]. The paralysis of GMC101 nematodes in

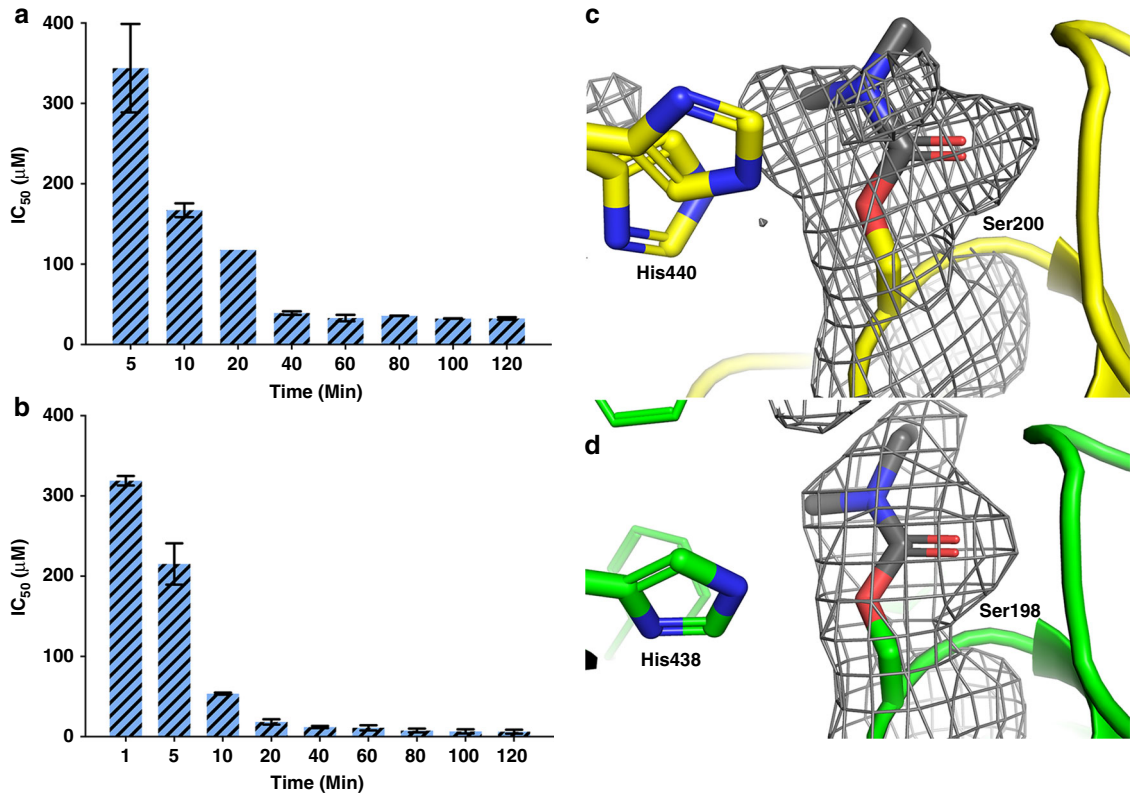

Fig. 5 Progressive inhibition of cholinesterases (ChEs) by **11** and X-ray crystal structures of ChEs after incubation with **11**. **a** Progressive inhibition of huAChE and **b** huBuChE by **11**. Values are mean ± SEM. **c** Close-up view of the active-site in the the X-ray structure of *Tc*AChE (PDB ID 6EUE; resolution 2.05 Å) and **d** huBuChE$_{CHO}$ (PDB ID 6EYF; resolution 2.60 Å) after incubation with **11**, showing carbamylated Ser200 and Ser198 residues, respectively. Carbon atoms are, respectively, represented in yellow in *Tc*AChE and green in huBuChE. The carbamyl moiety is in grey, oxygen atoms in red, and nitrogen atoms in blue. The $F_o - F_c$ electron density maps calculated by omitting carbamylated Ser200 in *Tc*AChE or carbamylated Ser198 and molecule **11** in huBuChE from the respective models are represented as grey mesh with a 3.0 σ contour

Table 4 Estimated BBB permeabilities of 8–11 and reference compound

Compounds[a]	Mean P_{app} (10^{-6} cm/s)	Carbamate P_{app}/Phenol P_{app}	Permeability category[b]
3-((Ethyl(methyl)carbamoyl)oxy)benzoic acid[c]	3.64	46.8	Moderate
10	9.15	8.09	High
9	22.3	0.93	High
11	33.6	1.28	High
Racemic rivastigmine (**8**)	33.8	1.31	High

[a]Values are mean of at least two independent experiments using an MDR1-MDCKII cell-based model. Replicate P_{app} values were within 5% of the mean. The test concentration was 2 μM with 2.5 h incubation. Pgp efflux ratios**:** 3-((ethyl(methyl)carbamoyl)oxy)benzoic acid, 0.50; **10**, 1.55**;** galantamine, 0.97; **9**, 0.72; donepezil, 0.82; **11**, 0.73; racemic rivastigmine (**8**), 0.76; (*S*)-rivastigmine [(*S*)-**8**], 0.75
[b]Low permeability: $P_{app} \leq 1.0$ ($\times 10^{-6}$ cm/s); Moderate permeability: $1.0 < P_{app} < 5.5$ ($\times 10^{-6}$ cm/s); High permeability: $P_{app} \geq 5.5$ ($\times 10^{-6}$ cm/s). The boundaries for low and high permeability categories are equivalent to 50 and 80% of the calculated fraction absorbed (Fa) in humans
[c]The synthesis of this compound is described in the Supplementary Methods

the presence of **3**, **5**, **10**, **11** and EGCG[26], was significantly delayed in comparison with that of untreated controls at 16, 20 and 24 h at 25 °C. These results are in keeping with NAP analogues **3** and **5** being among the most potent $A\beta_{42}$ fibrillation inhibitors identified in earlier in vitro studies, while **10** and **11** are rivastigmine analogues that produce **3** and **5**, respectively, upon decarbamylation. *C. elegans* has four *ace* genes, with *ace-1* and *ace-2* encoding for two distinct AChEs, ACE-1 and ACE-2, which comprise 95% of all AChE activity[44]. *Ace-1* is expressed in muscle cells, while *ace-2* is expressed in neurons, and carbamates are known to inhibit *C. elegans* AChEs[44–46]. In contrast to the activity of the novel compounds (**3**, **5**, **10** and **11**), racemic NAP (**1**) significantly delayed paralysis at 16 h, but no significant effect was observed at 20 or 24 h, when compared with the untreated controls. Furthermore, (*S*)-rivastigmine [(*S*)-**8**] displayed a significant, albeit relatively weak, delay of paralysis at 16 and 24 h, with no significant effect at 20 h, when compared with the untreated controls. To investigate the inherent toxicity of the compounds, *C. elegans* transgenic control strain CL2122 was also grown on media that was pre-spotted with 100 μL of 2 mM of compound (**1**–**3**, **5**, **9**, **10**, **11**, (*S*)-**8** or EGCG). No significant paralysis was observed over the time course of the experiment, except for EGCG and NAP analogue **3**, which displayed a minor degree of paralysis at 24 h (CL2122 strain + EGCG, fraction not paralysed 0.97, $p < 0.0056$ c.f. untreated CL2122, fraction not paralysed 1.0; CL2122 strain +**3**, fraction not paralysed 0.95, $p <$

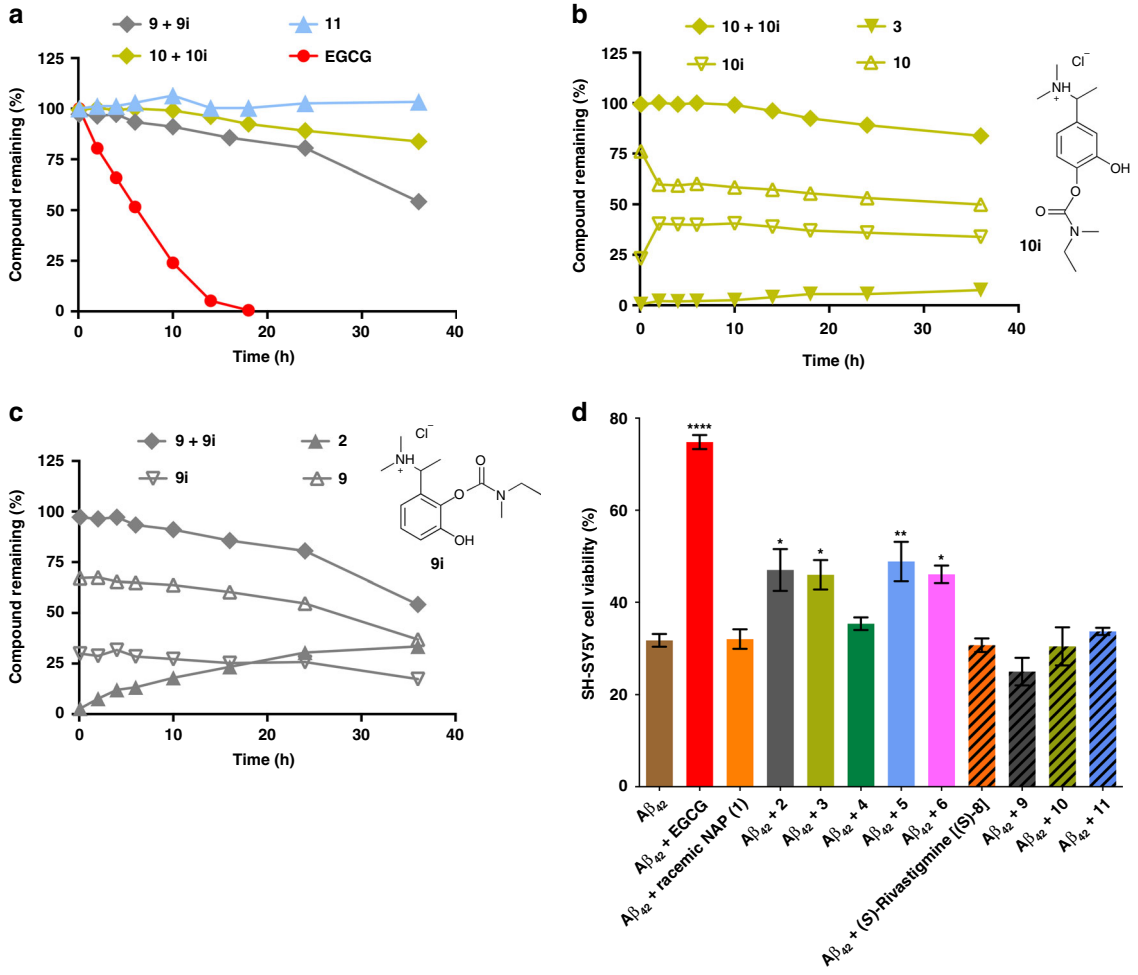

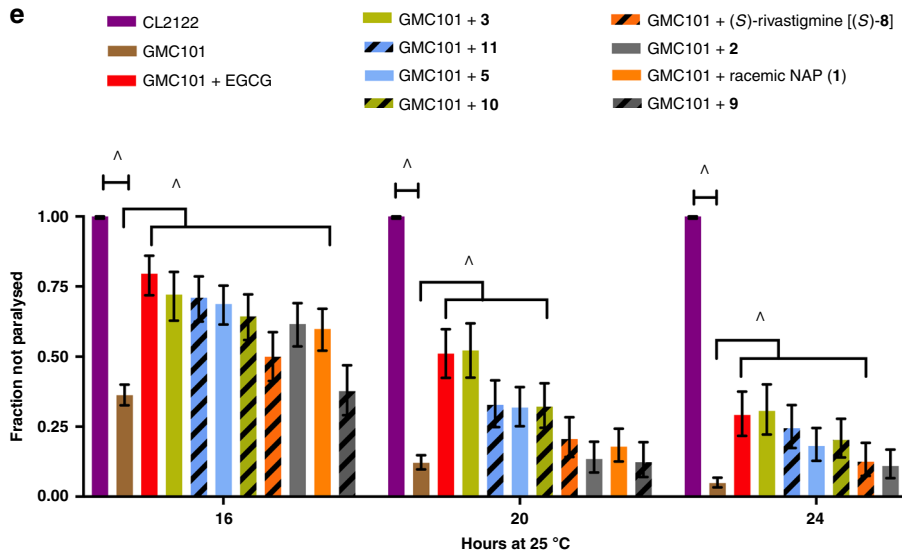

0.0056 c.f. untreated CL2122, fraction not paralysed 1.0) (Supplementary Fig. 24).

Discussion

EGCG exhibited potent inhibition of $A\beta_{42}$ fibrillation in vitro (Fig. 2a–k), and protected against $A\beta_{42}$-induced toxicity in both SH-SY5Y cells in vitro (Fig. 6d) and transgenic *C. elegans* strain GMC101 in vivo (Fig. 6e). However, EGCG has very low permeability across a MDR1-MDCKII cell-based model of the BBB (Table 2), and is rapidly degraded in phosphate buffer (Fig. 2l). To overcome these disadvantages of EGCG, which are a common trait of many polyphenols, we incorporated one or two additional hydroxy groups into the structure of the current AD drug rivastigmine, and its metabolite NAP (Figs. 1b and 3a). We hypothesised that this strategy would create a multifunctional molecule, with anti-ChE activity residing in the rivastigmine analogue, and EGCG-like anti-Aβ fibrillation activity attributed

Fig. 6 Chemical stabilities of carbamates and protection against $A\beta_{42}$-induced toxicity. **a**–**c** Chemical stabilities of epigallocatechin gallate (EGCG), **9**, **10** and **11** incubated over 36 h in pH 7.4 phosphate buffer at 23 °C. Time course showing estimated % compound remaining over 36 h for: **a** EGCG, **9** + structural isomer **9i**, **10** + structural isomer **10i** and **11**; **b** rivastigmine analogue **10**; and **c** rivastigmine analogue **9**. **d** Protection against $A\beta_{42}$-induced neurotoxicity. $A\beta_{42}$ alone, or in combination with compounds, was incubated in pH 7.4 phosphate buffer at 37 °C for 2 h, then added to SH-SY5Y cells and incubated for 48 h at 37 °C. The final concentrations of $A\beta_{42}$ and compounds were 3.9 and 5.0 μM, respectively. Values are % viability relative to cells unexposed to $A\beta_{42}$ and shown as the mean ± SEM of three independent experiments. $^{*}p < 0.05$, $^{**}p < 0.01$ and $^{****}p < 0.0001$ c.f. $A\beta_{42}$ control as determined by one-way analysis of variance (ANOVA) followed by Tukey's multiple comparisons test. **e** Protection against $A\beta_{42}$-induced toxicity in *C. elegans* at 25 °C. Plotted are the proportions of individuals not paralysed for untreated strains GMC101 and CL2122, and GMC101 grown in a petri dishes (30 × 15 mm) on media pre-spotted with 100 μL of 2 mM of compound. Values are the mean with upper and lower 95% confidence intervals, based on data pooled from three independent experiments: Control strain CL2122 ($n = 487$)[39], Aβ1–42 strain GMC101 ($n = 678$)[39], GMC101 strain + EGCG ($n = 137$)[39], GMC101 strain + racemic NAP (**1**) ($n = 179$), GMC101 strain + **2** ($n = 164$), GMC101 strain + **3** ($n = 111$), GMC101 strain + **5** ($n = 182$), GMC101 strain + (*S*)-rivastigmine [(*S*)-**8**] ($n = 136$), GMC101 strain + **9** ($n = 122$), GMC101 strain + **10** ($n = 143$), GMC101 strain + **11** ($n = 131$), where n = number of individuals assayed. Statistical significance was determined by an 11 × 2 Fisher's exact test for each time point, which gave overall p-values < 0.001. A series of 2 × 2 Fisher's exact tests were subsequently conducted for pairwise comparisons, applying the Bonferroni correction for multiple tests, with $p < 0.005$

to the NAP analogue, which would be released by the action of ChEs (Fig. 1a). Indeed, NAP analogues **2**, **3** and **5** emerged as very strong-to-moderate inhibitors of $A\beta_{42}$ fibrillation among the series of synthesised compounds (**1**–**7**) (Fig. 2a–k). Somewhat surprisingly, **2** and **5** showed high permeabilities, while **3** had moderate permeability, across an MDR1-MDCKII monolayer, in stark contrast to the very low permeabilities of EGCG and gallic acid (Table 2). These differences in permeabilities were rationalised in terms of the predicted hydrophilicities of the compounds and polarity-concealing intramolecular hydrogen bonding between the additional hydroxy group and the adjacent tertiary amine group of **2** and **5**, indicated by in silico modelling (Supplementary Tables 6 and 7). The results suggest that **2**, **3** and **5** could be suitable for direct administration to patients as polyphenolic NAP analogues, rather than in the form of carbamates (rivastigmine analogues). However, NAP analogues **2**, **3** and **5** exhibited substantial degradation in phosphate buffer (Fig. 2l), and we hypothesised that this problem could be overcome by carbamylation of one of their hydroxy groups, thus forming rivastigmine analogues that are less susceptible to auto-oxidation and imparting the molecules with anti-ChE activity. Indeed, rivastigmine analogues **9**–**11** were relatively stable in phosphate buffer (Fig. 6a–c), notwithstanding isomerization of **9** and **10**, and they were strong-to-moderate inhibitors of huAChE and huBuChE, albeit slightly less potent than rivastigmine (Table 3). These rivastigmine analogues (**9**–**11**) were pseudo-irreversible inhibitors of ChEs, which carbamylate the enzyme active-site serine residue with concomitant release of the NAP analogue from the active-site (Fig. 5a–d). Importantly, rivastigmine analogues **9**–**11** were estimated to have high BBB permeabilities according to the MDR1-MDCKII cell-based BBB model (Table 4), with slight differences in P_{app} that could be explained by compound hydrophilicity and polarity-concealing intramolecular hydrogen bonding predicted by in silico modelling (Supplementary Tables 6 and 7). Furthermore, rivastigmine analogues **10** and **11**, and their corresponding NAP analogues **3** and **5**, protected against $A\beta_{42}$-induced toxicity in both SH-SY5Y cells in vitro (Fig. 6d) and transgenic *C. elegans* strain GMC101 in vivo (Fig. 6e). Therefore, rivastigmine analogues **10** and **11** are prospective multifunctional drugs for AD, with putative AD-modifying properties.

Possible limitations of using rivastigmine analogues (e.g., **10** and **11**) to deliver NAP analogues (e.g., **3** and **5**) to the brain are mentioned in the Supplementary Discussion, including: (a) the potential for cholinergic toxicity to limit the achievable brain concentrations of the compounds; and (b) the possible oxidation of polyphenolic NAP analogues to potentially toxic quinones; although the rivastigmine analogues described in the current study are apparently protected from oxidation and, therefore, offer an opportunity for the brain delivery of an intact polyphenolic pharmacophore, as well as the investigation of its toxicity and of its effect on AD pathology in vivo.

Over the last two decades, there have been many reports of molecules that engage with multiple AD drug targets[47–49]. These multifunctional molecules, or multi-target-directed ligands (MTDLs) as they are often called, are constructed by combining multiple pharmacophores, each selected to interact with a different target, into a single chemical structure. The degree of integration of the pharmacophores ranges from conjugates containing separate pharmacophores joined by distinct linker groups, through structures containing distinct non-overlapping pharmacophores fused together without linkers, and on to merged pharmacophores with a high degree of structural overlay[50]. One of the most successful examples of this approach is the phase-2 drug candidate ladostigil (TV3326), which combines the pharmacophores of rivastigmine and the monoamine oxidase-B (MAO-B) inhibitor rasagiline[51]. The rivastigmine pharmacophore has also been combined with a metal chelating 8-hydroxyquinoline group to create a multifunctional molecule that releases a metal chelator as a result of decarbamylation by ChEs[52]. Additional MAO-A/B inhibitory activity was subsequently incorporated into the same ChE inhibitor-metal chelator system by including the rasagiline pharmacophore within the structure[53]. The pharmacophores of polyphenols and rivastigmine, which are the focus of this study, have been combined in several studies. In almost all cases the degree of integration was low, resulting in multifunctional molecules containing distinct non-overlapping pharmacophores and having much higher molecular weight than rivastigmine[54–57]. Furthermore, the basic amino group of rivastigmine, which is important for cation-π interactions with the active-site of ChEs[58] and is positively associated with CNS uptake[12–14], was absent in most of the molecules[54,56,57]. The only exception is the study of Li et al.[59], in which the 2-methoxyphenol pharmacophore of curcumin was merged with a structure similar to rivastigmine but containing modifications to the rivastigmine alkyl amino and carbamate moieties. In contrast, our study achieved multifunctionality through the very subtle addition of one hydroxy group to the otherwise unmodified rivastigmine structure, to incorporate potentially disease-modifying polyphenolic inhibition of Aβ fibrillation within a small druglike molecule very similar to rivastigmine. Despite the simplicity of this change, we were able to demonstrate its efficacy in vivo in an Aβ model of AD, whereas the majority of the aforementioned studies either did not examine the efficacy of the compounds in vivo[56,57,59], or they did not utilise an in vivo Aβ model of AD[54,55]. An important factor to consider, additionally, is the effect on stability and permeability of a molecule caused by introducing a polyphenolic moiety. The benefit of our rivastigmine analogues, unlike other

multifunctional analogues, which feature permanent polyphenolic groups[54,56,57], is that the polyphenol is only released after the carbamate group is cleaved by ChEs. This improves the stability and BBB permeability of the compound, as is demonstrated in our assays. It may also increase release of the polyphenol in the targeted regions of the AD brain. The strategies described in this study to deliver polyphenolic pharmacophores to the CNS for the treatment of AD could potentially be used for CNS delivery of polyphenols more generally.

Methods

Compound synthesis. See Supplementary Methods, Supplementary Tables 1 and 2 and Supplementary Figs. 1–4.

Compound stability. See Supplementary Methods, Supplementary Table 3 and Supplementary Figs. 5–17.

Inhibition of Aβ fibrillation. See Supplementary Methods and Supplementary Figs. 18–20.

Inhibition of cholinesterases. See Supplementary Methods, Supplementary Table 4 and Supplementary Fig. 21.

X-ray crystallography. See Supplementary Methods, Supplementary Table 5 and Supplementary Fig. 22.

Estimation of BBB permeability. See Supplementary Methods.

Molecular modelling. See Supplementary Methods and Supplementary Tables 6 and 7.

Inherent toxicity and protection against Aβ-induced toxicity. See Supplementary Methods and Supplementary Figs. 23 and 24.

Compound spectra. See Supplementary Figs. 25–122.

Reporting Summary. Further information on experimental design is available in the Nature Research Reporting Summary linked to this article.

Data availability

The data supporting the findings of this study are available within the article and its Supplementary Information file or from the corresponding author upon reasonable request. Structural data are available from the Protein Data Bank under accession numbers 6EUE for *Tc*AChE structure, 6EYF for huBuChE$_{CHO}$ and 6EZ2 for huBuChE$_{insect}$.

Received: 19 July 2018 Accepted: 18 February 2019
Published online: 22 March 2019

References

1. Scheltens, P. et al. Alzheimer's disease. *Lancet* **388**, 505–517 (2016).
2. Prince, M., Guerchet, M. & Prina, M. Policy brief for heads of government: the global impact of dementia, 2013–2050 (2013).
3. Selkoe, D. J. & Hardy, J. The amyloid hypothesis of Alzheimer's disease at 25 years. *EMBO Mol. Med.* **8**, 595–608 (2016).
4. Christensen, D. D. Changing the course of Alzheimer's disease: anti-amyloid disease-modifying treatments on the horizon. *Prim. Care Companion J. Clin. Psychiatry* **9**, 32–41 (2007).
5. Bastianetto, S., Yao, Z. X., Papadopoulos, V. & Quirion, R. Neuroprotective effects of green and black teas and their catechin gallate esters against β-amyloid-induced toxicity. *Eur. J. Neurosci.* **23**, 55–64 (2006).
6. Chan, S. et al. Metal chelation, radical scavenging and inhibition of $A\beta_{42}$ fibrillation by food constituents in relation to Alzheimer's disease. *Food Chem.* **199**, 185–194 (2016).
7. Ono, K., Hasegawa, K., Naiki, H. & Yamada, M. Anti-amyloidogenic activity of tannic acid and its activity to destabilize Alzheimer's β-amyloid fibrils in vitro. *Biochim. Biophys. Acta, Mol. Basis Dis.* **1690**, 193–202 (2004).
8. Schaffer, S. & Halliwell, B. Do polyphenols enter the brain and does it matter? Some theoretical and practical considerations. *Genes Nutr.* **7**, 99–109 (2012).
9. Yang, C. S., Sang, S., Lambert, J. D. & Lee, M. -J. Bioavailability issues in studying the health effects of plant polyphenolic compounds. *Mol. Nutr. Food Res.* **52**, S139–S151 (2008).
10. Lipinski, C. A., Lombardo, F., Dominy, B. W. & Feeney, P. J. Experimental and computational approaches to estimate solubility and permeability in drug discovery and development settings. *Adv. Drug Deliv. Rev.* **23**, 3–25 (1997).
11. Hitchcock, S. A. & Pennington, L. D. Structure− brain exposure relationships. *J. Med. Chem.* **49**, 7559–7583 (2006).
12. Ghose, A. K., Herbertz, T., Hudkins, R. L., Dorsey, B. D. & Mallamo, J. P. Knowledge-Based, Central Nervous System (CNS) Lead Selection and Lead Optimization for CNS Drug Discovery. *ACS Chem. Neurosci.* **3**, 50–68 (2012).
13. Rankovic, Z. CNS drug design: balancing physicochemical properties for optimal brain exposure. *J. Med. Chem.* **58**, 2584–2608 (2015).
14. Pajouhesh, H. & Lenz, G. R. Medicinal chemical properties of successful central nervous system drugs. *NeuroRx* **2**, 541–553 (2005).
15. Manach, C., Scalbert, A., Morand, C., Rémésy, C. & Jiménez, L. Polyphenols: food sources and bioavailability. *Am. J. Clin. Nutr.* **79**, 727–747 (2004).
16. Bolton, J. L., Trush, M. A., Penning, T. M., Dryhurst, G. & Monks, T. J. Role of quinones in toxicology. *Chem. Res. Toxicol.* **13**, 135–160 (2000).
17. Galati, G., Lin, A., Sultan, A. M. & O'Brien, P. J. Cellular and in vivo hepatotoxicity caused by green tea phenolic acids and catechins. *Free Radic. Biol. Med.* **40**, 570–580 (2006).
18. Gottwald, M. D. & Rozanski, R. I. Rivastigmine, a brain-region selective acetylcholinesterase inhibitor for treating Alzheimer's disease: review and current status. *Expert Opin. Invest. Drugs* **8**, 1673–1682 (1999).
19. Bar-On, P. et al. Kinetic and structural studies on the interaction of cholinesterases with the anti-Alzheimer drug rivastigmine. *Biochemistry* **41**, 3555–3564 (2002).
20. Bolognesi, M. L. et al. Design, synthesis, and biological evaluation of conformationally restricted rivastigmine analogues. *J. Med. Chem.* **47**, 5945–5952 (2004).
21. Cutler, N. et al. Dose-dependent CSF acetylcholinesterase inhibition by SDZ ENA 713 in Alzheimer's disease. *Acta Neurol. Scand.* **97**, 244–250 (1998).
22. Tashma, Z. Stigmines. In *Analogue-Based Drug Discovery* (eds. Fischer, J. & Ganellin, C. R.) 277–295 (Wiley-VCH, Weinheim, 2006).
23. Weinstock, M., Razin, M., Chorev, M. & Tashma, Z. Pharmacological Activity of Novel Anticholinesterase Agents of Potential Use in the Treatment of Alzheimer's Disease in *Alzheimer's and Parkinson's Disease* (eds. Fisher, A., Hanin, I. & Lachman, C.) 539–549 (Plenum Press, New York, 1986).
24. Rakonczay, Z. Potencies and selectivities of inhibitors of acetylcholinesterase and its molecular forms in normal and Alzheimer's disease brain. *Acta Biol. Hung.* **54**, 183–189 (2003).
25. Enz, A., Boddeke, H., Gray, J. & Spiegel, R. Pharmacologic and clinicopharmacologic properties of SDZ ENA 713, a centrally selective acetylcholinesterase inhibitor. *Ann. N. Y. Acad. Sci.* **640**, 272–275 (1991).
26. Kantham, S. et al. Effect of the biphenyl neolignan honokiol on Aβ42-induced toxicity in *Caenorhabditis elegans*, Aβ42 Fibrillation, cholinesterase activity, DPPH radicals, and Iron(II) chelation. *ACS Chem. Neurosci.* **8**, 1901–1912 (2017).
27. Levine, H. T. T interaction with synthetic Alzheimer's disease β-amyloid peptides: Detection of amyloid aggregation in solution. *Protein Sci.* **2**, 404–410 (1993).
28. Shen, D. et al. Novel cell-and tissue-based assays for detecting misfolded and aggregated protein accumulation within aggresomes and inclusion bodies. *Cell Biochem. Biophys.* **60**, 173–185 (2011).
29. Arosio, P., Cukalevski, R., Frohm, B., Knowles, T. P. & Linse, S. Quantification of the concentration of Aβ42 propagons during the lag phase by an amyloid chain reaction assay. *J. Am. Chem. Soc.* **136**, 219–225 (2013).
30. Bakos, E. et al. Functional multidrug resistance protein (MRP1) lacking the N-terminal transmembrane domain. *J. Biol. Chem.* **273**, 32167–32175 (1998).
31. Di, L., Kerns, E. H. & Carter, G. T. Strategies to assess blood-brain barrier penetration. *Expert Opin. Drug Discov.* **3**, 677–687 (2008).
32. Deora, G. S. et al. Multifunctional analogs of kynurenic acid for the treatment of Alzheimer's disease: synthesis, pharmacology, and molecular modeling studies. *ACS Chem. Neurosci.* **8**, 2667–2675 (2017).
33. Alex, A., Millan, D. S., Perez, M., Wakenhut, F. & Whitlock, G. A. Intramolecular hydrogen bonding to improve membrane permeability and absorption in beyond rule of five chemical space. *Med. Chem. Comm.* **2**, 669–674 (2011).
34. Koh, H. L., Go, M. L., Ngiam, T. & Mak, J. W. Conformational and structural features determining in vitro antimalarial activity in some indolo[3,2-c] quinolines, anilinoquinolines and tetrahydroindolo[3,2-d]benzazepines. *Eur. J. Med. Chem.* **29**, 107–113 (1994).
35. Madrid, P. B., Liou, A. P., DeRisi, J. L. & Guy, R. K. Incorporation of an intramolecular hydrogen-bonding motif in the side chain of 4-aminoquinolines enhances activity against drug-resistant *P. falciparum*. *J. Med. Chem.* **51**, 699–699 (2008).

36. Gemma, S. et al. Mimicking the intramolecular hydrogen bond: synthesis, biological evaluation, and molecular modeling of benzoxazines and quinazolines as potential antimalarial agents. *J. Med. Chem.* **55**, 10387–10404 (2012).
37. Dewick, P. M. *Medicinal Natural Products: A Biosynthetic Approach 3rd Edition*. (John Wiley & Sons, Chichester, West Sussex, United Kingdom 2002).
38. Sang, S., Buckley, B., Ho, C. -T. & Yang, C. S. Autoxidative quinone formation in vitro and metabolite formation in vivo from tea polyphenol (−)-epigallocatechin-3-gallate: studied by real-time mass spectrometry combined with tandem mass ion mapping. *Free Radic. Biol. Med.* **43**, 362–371 (2007).
39. Oliveira, C. M., Ferreira, A. C. S., De Freitas, V. & Silva, A. M. Oxidation mechanisms occurring in wines. *Food Res. Int.* **44**, 1115–1126 (2011).
40. Hardy, J. & Allsop, D. Amyloid deposition as the central event in the aetiology of Alzheimer's disease. *Trends Pharmacol. Sci.* **12**, 383–388 (1991).
41. Fändrich, M. Oligomeric intermediates in amyloid formation: structure determination and mechanisms of toxicity. *J. Mol. Biol.* **421**, 427–440 (2012).
42. McColl, G. et al. Utility of an improved model of amyloid-beta ($A\beta_{1-42}$) toxicity in Caenorhabditis elegans for drug screening for Alzheimer's disease. *Mol. Neurodegener.* **7**, 57 (2012).
43. Fay, D. S., Fluet, A., Johnson, C. J. & Link, C. D. In vivo aggregation of beta-amyloid peptide variants. *J. Neurochem.* **71**, 1616–1625 (1998).
44. Combes, D., Fedon, Y., Grauso, M., Toutant, J. -P. & Arpagaus, M. Four Genes Encode Acetylcholinesterases in the Nematodes Caenorhabditis elegans and Caenorhabditis briggsae. cDNA Sequences, Genomic Structures, Mutations and in vivo Expression. *J. Mol. Biol.* **300**, 727–742 (2000).
45. Melstrom, P. C. & Williams, P. L. Reversible AChE inhibitors in C. elegans vs. rats, mice. *Biochem. Biophys. Res. Commun.* **357**, 200–205 (2007).
46. Chaudhaery, S. S. et al. Novel carbamates as orally active acetylcholinesterase inhibitors found to improve scopolamine-induced cognition impairment: pharmacophore-based virtual screening, synthesis, and pharmacology. *J. Med. Chem.* **53**, 6490–6505 (2010).
47. Cavalli, A. et al. Multi-target-directed ligands to combat neurodegenerative diseases. *J. Med. Chem.* **51**, 347–372 (2008).
48. Dias, K. S. & Viegas, C. Jr. Multi-target directed drugs: a modern approach for design of new drugs for the treatment of Alzheimer's Disease. *Curr. Neuropharmacol.* **12**, 239–255 (2014).
49. de Freitas Silva, M., Dias, K. S. T., Gontijo, V. S., Ortiz, C. J. C. & Viegas, C. Jr. Multi-target directed drugs as a modern approach for drug design towards alzheimer's disease: An update. *Curr. Med. Chem.* **25**, 3491–3525 (2018).
50. Morphy, R. & Rankovic, Z. Designed multiple ligands. An emerging drug discovery paradigm. *J. Med. Chem.* **48**, 6523–6543 (2005).
51. Weinstock, M. et al. TV3326, a novel neuroprotective drug with cholinesterase and monoamine oxidase inhibitory activities for the treatment of Alzheimer's disease in *Advances in Research on Neurodegeneration* (eds. Riederer, P. et al.) 157–169 (Springer, Vienna, 2000).
52. Zheng, H., Youdim, M. B. H. & Fridkin, M. Site-activated multifunctional chelator with acetylcholinesterase and neuroprotective−neurorestorative moieties for Alzheimer's therapy. *J. Med. Chem.* **52**, 4095–4098 (2009).
53. Zheng, H., Youdim, M. B. H. & Fridkin, M. Site-activated chelators targeting acetylcholinesterase and monoamine oxidase for Alzheimer's therapy. *ACS Chem. Biol.* **5**, 603–610 (2010).
54. Sang, Z. -p et al. Design, synthesis, and biological evaluation of scutellarein carbamate derivatives as potential multifunctional agents for the treatment of Alzheimer's disease. *Chem. Biol. Drug. Des.* **86**, 1168–1177 (2015).
55. Sang, Z. -p et al. Multifunctional scutellarin–rivastigmine hybrids with cholinergic, antioxidant, biometal chelating and neuroprotective properties for the treatment of Alzheimer's disease. *Bioorg. Med. Chem.* **23**, 668–680 (2015).
56. Chen, Z. et al. Discovery of novel rivastigmine-hydroxycinnamic acid hybrids as multi-targeted agents for Alzheimer's disease. *Eur. J. Med. Chem.* **125**, 784–792 (2017).
57. Nesi, G. et al. Nature-based molecules combined with rivastigmine: A symbiotic approach for the synthesis of new agents against Alzheimer's disease. *Eur. J. Med. Chem.* **141**, 232–239 (2017).
58. Sussman, J. L. & Silman, I. Acetylcholinesterase: structure and use as a model for specific cation—protein interactions. *Curr. Opin. Struct. Biol.* **2**, 721–729 (1992).
59. Li, Y. et al. Design, synthesis and evaluation of rivastigmine and curcumin hybrids as site-activated multitarget-directed ligands for Alzheimer's disease therapy. *Bioorg. Med. Chem.* **22**, 4717–4725 (2014).

Acknowledgements

The following financial support is gratefully acknowledged: UQ School of Pharmacy funding (M.-O.P. and B.P.R.); and DGA/SSA BioMedef contract PDH-2 NRBC-3-C-3201 (X.B.). S.N.D., S.C., S.K., J.A.M., S.K.V., B.Y.S. and Z.D.N. thank UQ and the Australian Government for PhD scholarships. S.N.D. thanks UQ for a GSITA travel grant.

Author contributions

S.N.D., B.Y.S., B.P.R. and R.P.M. designed the chemical synthesis and interpreted the chemical analysis data. S.N.D. and B.Y.S. conducted the chemical synthesis. S.N.D. and J.A.M. conducted the ChE activity assays. S.N.D. conducted the SH-SY5Y cell-based assay, and interpreted the results of the cell-based BBB model assay. S.N.D. and S.K.V conducted Aß fibrillation assays and the chemical stability assay. S.C. conducted transmission electron microscopy. J.A.M. conducted the molecular modelling. E.D.M. and X.B. conducted X-ray crystallography. E.D.M., I.S., J.L.S., M.W. and X.B. interpreted the X-ray crystallography results. M.-O.P. and Z.D.N. interpreted the SH-SY5Y cell-based assay results. S.C. and S.K. conducted the *C. elegans* Aß toxicity assay. G.M. interpreted the results of the *C. elegans* Aß toxicity assay. X.B. and I.S. produced huBuChE and *Tc*AChE. B.P.R. conceived and designed the study, and participated in the processing of data and interpretation of results. B.P.R., S.N.D., J.A.M. and X.B. wrote the manuscript. All of the authors read, edited and approved the final version of the manuscript.

Additional information

Supplementary information accompanies this paper at https://doi.org/10.1038/s42004-019-0133-4.

Competing interests: A provisional patent application is pending on the chemical identity of compounds described in this manuscript (Australian application number: 2018904090; Filing date: 29 October, 2018; Applicant: The University of Queensland).

Reprints and permission information is available online at http://npg.nature.com/reprintsandpermissions/

Publisher's note: Springer Nature remains neutral with regard to jurisdictional claims in published maps and institutional affiliations.